EvoDevo

RESEARCH Open Access

A subset of conserved phagocytic genes are likely used for the intracellular theft of cnidarian stinging organelles in nudibranch gastropods

Jessica A. Goodheart[1,2,6*], Rose Fiorenza[2], Robin Rio[2], Rebecca N. Lopez-Anido[1,6], Noah J. Martin[3,4,5], Timothy J. Herrlinger[3], Rebecca D. Tarvin[3,4] and Deirdre C. Lyons[2]

Abstract

Background Phagocytosis is a universal physiological process in eukaryotes with many important biological functions. In nudibranch gastropods, a novel form of phagocytosis called nematocyst sequestration is specialized for the uptake of venomous stinging organelles stolen from their cnidarian prey. This process is highly selective. Here we use the emerging model nudibranch species *Berghia stephanieae* and *Hermissenda opalescens* to identify genes enriched within the body regions where nematocyst sequestration occurs, and investigate how the expression profile of phagocytosis, immune, and digestive genes differs between nematocyst-sequestering regions relative to those where other phagocytic functions occur.

Results We identified 166 genes with significantly higher expression in sequestering regions in *B. stephanieae*, including genes associated with development, membrane transport, and metabolism. Of these, at least 31 overlap with transcripts upregulated in *H. opalescens* sequestering tissues. Using hybridization chain reaction in situs, we show that at least two of these genes were localized to sequestering cells in *B. stephanieae*, including a putative C-type lectin receptor and a collagen. Genes annotated with phagocytosis, digestion, or immunity GO terms were often expressed in both sequestering and non-sequestering tissues, suggesting that they may also play a role in sequestration processes.

Conclusion Our results suggest that phagocytosis genes likely play a role in the sequestration phenotype, and that a small subset of genes (e.g., collagen) may play unique functions yet to be uncovered. We also show that genes categorized as functioning in endocytosis, immunity, and digestion have lower overall expression in sequestering tissues, supporting the hypothesis that sequestering tissues show a narrowing of function compared to digestive tissues. This study lays the foundation for further inquiry into mechanisms of organelle sequestration in nudibranchs and other organisms.

Keywords Nematocyst, Sequestration, Phagocytosis, Immunity, Defense, Novelty

*Correspondence:
Jessica A. Goodheart
jgoodheart@amnh.org
Full list of author information is available at the end of the article

© The Author(s) 2025. **Open Access** This article is licensed under a Creative Commons Attribution 4.0 International License, which permits use, sharing, adaptation, distribution and reproduction in any medium or format, as long as you give appropriate credit to the original author(s) and the source, provide a link to the Creative Commons licence, and indicate if changes were made. The images or other third party material in this article are included in the article's Creative Commons licence, unless indicated otherwise in a credit line to the material. If material is not included in the article's Creative Commons licence and your intended use is not permitted by statutory regulation or exceeds the permitted use, you will need to obtain permission directly from the copyright holder. To view a copy of this licence, visit http://creativecommons.org/licenses/by/4.0/.

Background

Phagocytosis—the process by which certain living cells ingest or engulf other cells or particles—is a universal physiological process across eukaryotes [1]. Phagocytosis is critical for basic biological functions including innate and adaptive immune responses, tissue homeostasis, and intracellular digestion [2, 3]. Thus far, much of the work on phagocytosis has focused on "professional" phagocytes (i.e., cells where phagocytosis is the primary function, such as macrophages and neutrophils) from in vitro mammalian models and cell lines [4–6], along with a few other vertebrates [7] and ecdysozoans such as *Drosophila* [8] and *C. elegans* [9]. These studies largely center on immunity and homeostasis (anti-pathogen and clearance phagocytosis [10]). However, other phagocytes, such as digestive cells that perform intracellular digestion, are also common across Metazoa [11]. Some unusual versions of phagocytosis also exist among metazoans, such as the theft of stinging organelles (i.e., nematocysts) from cnidarian prey, termed nematocyst sequestration [12, 13]. In this study, we use nematocyst sequestration in nudibranch gastropods to investigate how generalist phagocytes might be modified for novel functions.

In nudibranchs, nematocyst sequestration takes place at the distal edges of the digestive tract in an organ called the cnidosac, and within an evolutionarily novel cell type called a cnidophage [13–15]. This organ is at the distal end of the ceras (Fig. 1), which is made up of a number of tissue types, including neurosensory, epidermal, muscle, and digestive [16, 17]. Some cell types are known to be found distributed across the ceras, including sensory cilial tufts and hemocytes (Fig. 1C). In the cnidosac, sequestered nematocysts appear to provide defensive and prey capture functions [15, 16, 18, 19] for the nudibranchs, as they do in their native cnidarians [20, 21], but we know very little about how they are phagocytosed and stored. Previous research on phagocytosis in mollusks has focused on the bivalve immune response (e.g., within hemocyte cells [17, 22]), including environmental effects on phagocytosis and immunity, but have rarely extended to molecular mechanisms [23–26]. Furthermore, mollusk immune cells are primarily generalists with regard to foreign targets, often expressing many different receptors in each cell [27]. In contrast, cnidophages exhibit a highly selective form of phagocytosis that exclusively targets nematocysts separated from their original cnidarian nematocyte cell (Fig. 1C) [14]. Various phagocytic cells, including those involved in immunity (e.g., hemocytes), have also been previously implicated in functions similar to nematocyst sequestration, like squid–Vibrio [28], cnidarian–dinoflagellate [29], plant–bacterial [30] and insect–bacterial [31] symbioses. We hypothesize that self–nonself programs similar to those used in symbiosis are also used to target nematocysts for sequestration in nudibranchs.

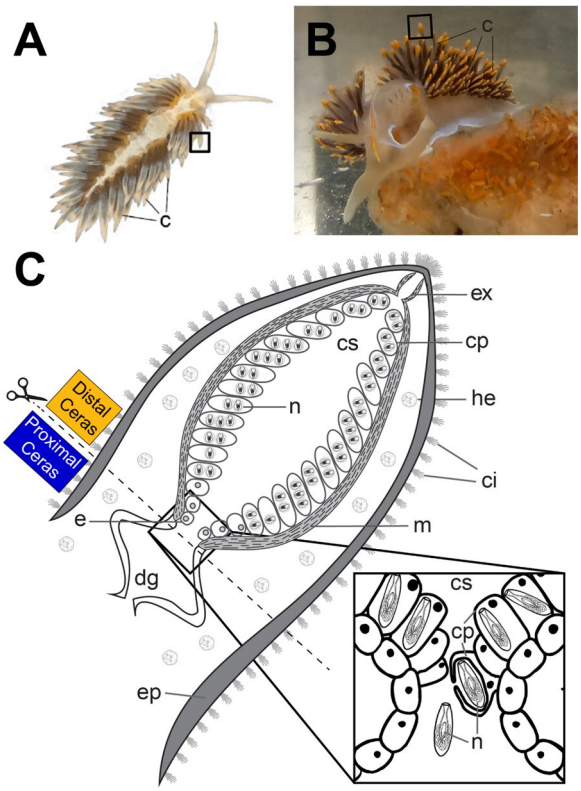

Fig. 1 Specialized phagocytosis (i.e., nematocyst sequestration) of nematocysts in (**A**) *Berghia stephanieae,* and (**B**) *Hermissenda opalescens*. C Generalized cnidosac schematic modified from Goodheart et al. 2018 [14] (under CC BY 4.0 Creative Commons License) highlighting the main features of the cnidosac. (*Inset*) Nematocysts (n) are phagocytosed by cnidophages inside the cnidosac (cs). Abbreviations: c, cerata; ci, cilia tufts; cp, cnidophage; cs, cnidosac; dg, digestive gland; e, entrance to the cnidosac; ep, epithelium; ex, exit from the cnidosac; he, hemocytes; m, musculature; n, nematocysts

Here we use the emerging model nudibranch species *Berghia stephanieae* (Valdés, 2005) [32] (Fig. 1A) and the opalescent nudibranch *Hermissenda opalescens* (Cooper, 1863) (Fig. 1B) to identify candidate genes and processes used by cnidophages to steal stinging organelles. *B. stephanieae* and *H. opalescens* are both aeolid nudibranchs (i.e., within the superfamily Aeolidioidea) in the sister families Aeolidiidae and Facelinidae, respectively [33–35], that are known to sequester nematocysts in cnidosacs at the tips of their cerata [14]. *B. stephanieae* is a tropical species described from the Florida Keys [32], and is known to only eat *Exaiptasia diaphana* anemones [36]. *H. opalescens*, on the other hand, is a generalist species that eats various cnidarians and non-cnidarians and ranges from Baja California

to temperate coastal California [37]. For both species, we compare the expression of phagocytosis, immune, and digestive genes between nematocyst-sequestering regions (Distal Cerata) and non-sequestering digestive regions (Proximal Cerata) in cerata tissues to evaluate how these genes may have been modified within the specialized cnidophages. The molecular machinery necessary for phagocytosis often includes a diverse array of recognition receptors, particle internalization proteins, and phagosome maturation proteins [38–40]. We would therefore expect some mechanistic conservation in the phagocytic processes of cnidophage cells compared to other digestive cell types. However, we do not expect all molecular signatures of traditional phagocytes to be present in the cnidosac, because cnidophages must identify nematocysts using a more specific form of target recognition [36], and phagosome maturation may be arrested to prevent nematocyst degradation. Instead, we hypothesize that we would find a narrowing of phagocytic, digestive, and immune function in cnidophages compared to other, more broad phagocytic tissues such as the digestive system, and that the cnidosac may express genes specific to targeting and engulfment of nematocysts. We predict that this specialization will be reflected in the downregulation of phagocytosis, digestion, or immunity gene expression in sequestering tissues.

Results

Differential expression across cerata tissues

The results obtained from each of the two species were collected under different experiments, so we present them separately here. For *B. stephanieae*, we used existing RNA-seq samples [41] for the distal and proximal cerata (three of each) to perform our analyses, where the distal cerata were separated from proximal cerata just proximal to entrance of the cnidosac (Fig. 1C). The primary difference between the two regions is that the Distal Ceras contains the cnidosac, or the organ for nematocyst sequestration, and the Proximal Ceras contains primarily digestive tissues. The number of read pairs ranged from 23.7 million (SRX21326248, Distal Ceras) to 28.8 million (SRX8599772, Proximal Ceras) across all six samples ($\bar{x} = 27.1 \pm 2.3$ million reads per sample; Tables 1 and S1). On average, 75.9% (± 4.3%) of read pairs mapped uniquely to the *B. stephanieae* genome, and mapping percentage ranged from 68.5% of read pairs (SRX21326249, Proximal Ceras) to 80.6% of read pairs (SRX8599773, Distal Ceras). We identified expression (counts > 10 across all tissues [42]) in ~ 86.1% of genes (21,498 out of 24,960 predicted genes) in the *B. stephanieae* genome. Genes with a Log2 Fold Change > 2 and adjusted p-value < 0.05 were considered upregulated in a given tissue. Distal and Proximal Ceras tissues were found to have distinct expression profiles, though there were many similarities (Figs. S1, S2), including genes associated with endocytosis and phagocytosis (Table S2). We identified 166 genes with significantly higher expression in the Distal Ceras, including genes often associated with membrane structure and reorganization, such as collagen, actin, and alpha-tubulin, genes associated with lysosome activity, such as cathepsin L and battenin, and genes associated with receptor-mediated endocytosis, such as C-type lectin macrophage mannose receptors and a sortilin-related receptor (Table S3). By contrast, our analysis identified 458 genes with significantly lower expression in the Distal Ceras, including many putative phagocytosis genes such as C1q-like proteins and antigen-like proteins (Table S5). However, we also found extensive overlap in the genes expressed in the Distal Ceras and Proximal Ceras in *B. stephanieae* (~ 87% of the total genes expressed, Fig. S3), including many other phagocytosis genes such as non-opsonic receptors, activation of internalization, phagosome formation and activation, phagocytosis-related responses, and phagocytosis efficiency genes (Table S2).

The constructed reference transcriptome for *Hermissenda opalescens* included 19,347 transcripts, with an average sequence length of 1202 nucleotides and an N50 of 1839 bp. The metazoa_odb10 BUSCO analysis indicated 75.3% completeness (C: 75.3% [S:

Table 1 Mapping results for *Berghia stephanieae* samples

SRA number	Label	Tissue	Total reads	Uniquely mapped reads	Uniquely mapped reads (%)
SRX8599773	D1	Distal Ceras	28,580,383	23,029,649	80.58
SRX21326248	D2	Distal Ceras	23,709,907	18,855,667	79.53
SRX21326247	D4	Distal Ceras	24,537,004	18,253,506	74.39
SRX8599772	P1	Proximal Ceras	28,817,227	21,824,061	75.73
SRX21326250	P2	Proximal Ceras	28,291,793	21,665,281	76.58
SRX21326249	P3	Proximal Ceras	28,539,632	19,534,354	68.45

71.4%, D: 3.9%], *F*: 10.6%, *M*: 14.1%, *n*: 954). RNA-seq samples for the distal and proximal cerata used for differential expression analysis ranged from 41.2 million (SRR32330747, Distal Ceras) to 96.5 million (SRR32330750, Distal Ceras) read pairs ($\bar{x} = 27.1 \pm 2.3$ million reads per sample; Tables 2 and S1). On average, mapping rates were relatively low (Tables 1, 2), with 42.1% (± 9.1%) of read pairs mapped uniquely to the existing *H. opalescens* transcriptome, and mapping percentage ranging from 26.8% of read pairs (SRR32330748, Proximal Ceras) to 58.7% of read pairs (SRR32330742, Distal Ceras). Due to these low mapping rates, and because *H. opalescens* data were more variable compared to our results in *B. stephanieae* (Fig. S3-S6), we used the *Hermissenda opalescens* results as a comparison to our findings in *B. stephanieae* rather than focusing our deep analysis efforts in this species. In *H. opalescens,* a total of 191 transcripts were found to be upregulated in the Distal Ceras, which were clustered within 96 orthologous groups by our OrthoFinder analysis. Twenty-seven (27) of these orthologous groups (containing 48 *H. opalescens* transcripts and 31 *B. stephanieae* genes) were found to be upregulated in the Distal Ceras in both species (Fig. 2A, Table 3). The transcripts upregulated in the *H. opalescens* Distal Ceras include those implicated in phagocytosis, including those annotated as Collagen alpha-1(VIII) chain, Pleckstrin homology domain-containing genes multiple solute carrier transporter genes, and a C-type lectin macrophage mannose receptor.

Confirmed expression of upregulated genes in *B. stephanieae*

To further localize gene expression for a subset of genes (Table 3), we used in situ hybridization chain reaction (HCR) at different stages of cerata development in *B. stephanieae* [43]. First, we examined the spatial expression of a known cnidophage marker in *B. stephanieae*, *bscola8a1* (OG0044763; annotated as Collagen alpha-1 VIII), and that of a putative cnidophage marker *bsclect* (OG0000337; annotated as c-type lectin) in both juveniles and adults. The expression pattern of *bscola8a1* was described in juveniles previously [41]. Prior to the formation of cerata buds, we did not detect any expression of *bsclect* or *bscola8a1* (Fig. 3A, B). In later staged juvenile (2–3 days post-feeding) [36], we detected co-expression of *bsclect* and *bscola8a1* in the cnidosac at the onset of cerata development (Fig. 3C, D). Both *bsclect* and *bscola8a1* appear to have restricted expression in the cnidosac (Fig. 3C), with *bscola8a1* exhibiting a relatively stronger signal than *bsclect* (Fig. 3D). To detect expression at a finer cellular level in the adult *B. stephanieae*, we conducted HCR on paraffin-sectioned cerata tissue. We identified co-expression of *bsclect* and *bscola8a1* in cnidophages within the cnidosac of adult *B. stephanieae* (Fig. 3E, F), with *bscola8a1* again showing a stronger signal than *bsclect*. Together we found co-localization of *bsclect* and *bscola8a1* within the cnidosac at multiple stages of cerata development (Fig. 3C–F).

To examine spatial expression of putative digestive gland genes, we selected *bsferritin* (jg36533; annotated as soma ferritin) and *bsbhmt* (jg32975; annotated as betaine–homocysteine S-methyltransferase 1) based on their

Table 2 Mapping results for *Hermissenda opalescens* samples

SRA number	Label	Tissue	Total reads	Uniquely mapped reads	Uniquely mapped reads (%)
SRR32330756	C_Ho057_cni	Distal Ceras	70,012,800	24,706,211	35.29
SRR32330734	C_Ho057_sub	Proximal Ceras	91,079,470	32,571,496	35.76
SRR32330728	C_R0901_cni	Distal Ceras	78,078,142	35,270,108	45.17
SRR32330755	C_R0901_sub	Proximal Ceras	60,542,912	30,850,728	50.96
SRR32330753	C_R0911_cni	Distal Ceras	77,359,288	32,280,450	41.73
SRR32330752	C_R0911_sub	Proximal Ceras	79,886,914	40,101,134	50.20
SRR32330750	N_Ho046_cni	Distal Ceras	96,459,888	37,135,312	38.50
SRR32330748	N_Ho046_sub	Proximal Ceras	68,441,684	18,341,937	26.80
SRR32330747	N_Ho047_cni	Distal Ceras	41,163,084	13,379,319	32.50
SRR32330744	N_Ho047_sub	Proximal Ceras	72,799,194	21,666,189	29.76
SRR32330742	N_R0900_cni	Distal Ceras	66,143,210	38,818,808	58.69
SRR32330740	N_R0900_sub	Proximal Ceras	64,862,456	31,872,321	49.14
SRR32330738	N_R0909_cni	Distal Ceras	64,376,370	29,957,916	46.54
SRR32330737	N_R0909_sub	Proximal Ceras	58,707,980	29,718,125	50.62

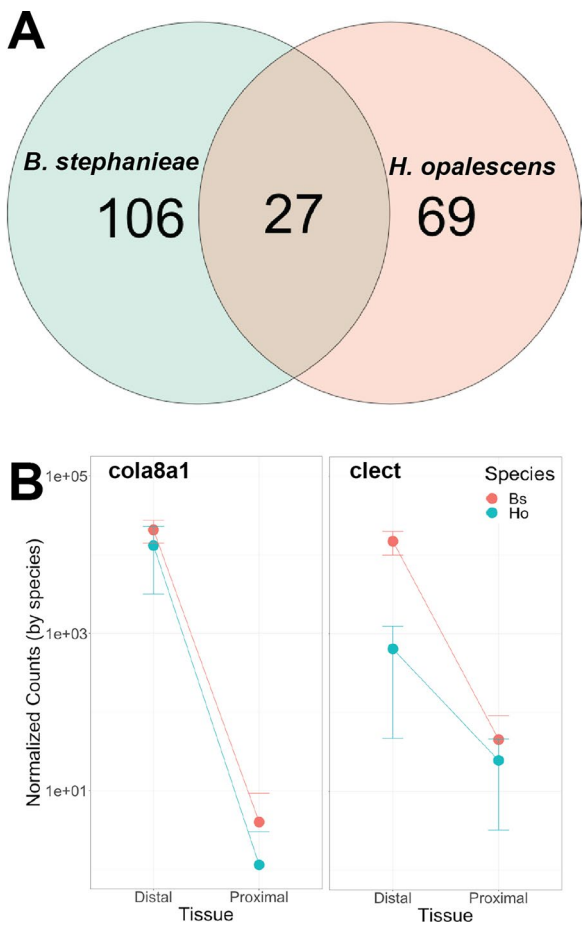

Fig. 2 Select *Hermissenda* and *Berghia* gene expression comparisons for genes upregulated in the Distal Ceras. **A** Venn diagram indicating the proportion of orthologous groups containing genes upregulated in the Distal Ceras overlapped between species. **B** Plots showing gene expression levels between the distal and proximal ceras for two orthologous phagocytosis genes in *B. stephanieae* and *H. opalescens*, including OG0044673 (Collagen alpha-1 chain, or cola8a1) and OG0000337 (macrophage mannose receptor 1, or clect). Expression profiles for these two genes are shown in Fig. 3

upregulation in proximal cerata tissue from our differential expression analysis and their putative role in digestion [44] and metabolism [45], respectively. During early juvenile development (prior to the formation of cerata), we detected strong expression of *bsferritin* in the anterior portion of the digestive gland (Fig. 4A-B). In contrast, we detected very weak expression of *bsbhmt* in the posterior digestive gland tissue (Fig. 4C, D). Further along in juvenile development (2–3 days post-feeding) [36], we found expression of both *bsferritin* and *bsbhmt* throughout the entire juvenile digestive gland (Fig. 4E–H). We did not detect any expression of *bsferritin* nor *bsbhmt* in the distal cerata where the cnidosac is located (Fig. 4F', H').

To identify any background fluorescence and/or hairpin trapping, we conducted HCR with negative controls that were incubated without any HCR probes (Fig. S7). We found that both 546 and 647 hairpins get trapped in epidermal tissue, and this is particularly prominent in paraffin-sectioned adult tissue (Fig. S7C–C").

Predicted functional changes in the Distal Ceras

We predicted that a narrowing of function would occur in the Distal Ceras resulting in a downregulation of phagocytosis, digestion, or immunity genes in sequestering tissues. To test this hypothesis, we investigated the primary functions associated with GO terms of genes upregulated in the Distal Ceras (Table S5) compared to those downregulated in the Distal Ceras (Table S6) in *B. stephanieae*. Those upregulated in the Distal Ceras included some terms that make sense for cnidosac function, like transmembrane transport (Fig. 5A), but also included some very specific metabolic terms such as lactone metabolic process or cellular lipid metabolic process. The primary GO terms associated with genes downregulated in the Distal Ceras include those associated with immune response, endocytosis, and digestion (Table S6; Fig. 5B).

We further investigated genes related to digestion (GO:0007586), endocytosis (GO:0006897), and immune response (GO:0006955) GO terms by comparing normalized and transformed counts (see Methods for details) for all genes or only differentially expressed (DE) genes. We found that in these GO terms, the differentially expressed sets of genes were on average expressed at a lower level in the Distal versus Proximal Ceras (Fig. 6). When comparing all orthologous genes across the Distal and Proximal Ceras, we found that these genes are not more likely to be up- or down-regulated in the Distal Ceras (Fig. 6A–C). However, we noted a clear pattern of directionality in differentially expressed genes, where these genes were more likely to be downregulated in the Distal Ceras compared to the Proximal Ceras (Fig. 6D–F).

Discussion

Phagocytosis, a conserved process for ingesting large particles, has been described largely based on the function of immune cells in a few major model systems [46], and the extent to which these components are conserved or have diverged across the vast majority of metazoan diversity is not fully understood. Mollusk (and particularly gastropod) immune cells and phagocytes are especially useful for the study of phagocytosis, because many diseases, including schistosomiasis (caused by flatworms), can be indirectly transmitted to humans by these animals [47]. Mollusk models have also long been advantageous in studying cell types, disease, and basic cellular processes [48, 49].

Table 3 Shared upregulated genes in the Distal Cerata of *B. stephanieae* and *H. opalescens* clustered into orthologous groups.

Orthogroup	log2 fold change	Database IDs	Protein names
OG0012058	– 16.333771	NA	NA
OG0000271	– 13.243509	O16025	Allene oxide synthase-lipoxygenase protein [Includes: Allene oxide synthase (AOS) (EC 4.2.1.-) (Hydroperoxidehydrase); Arachidonate 8-lipoxygenase (EC 1.13.11.40)]
OG0044673	– 12.345893	Q7LZR2	Collagen alpha-1(VIII) chain
OG0018973	– 10.802407	XP_045194129.1	NA
OG0000337	– 8.396657	P22897	Macrophage mannose receptor 1 (MMR) (C-type lectin domain family 13 member D) (C-type lectin domain family 13 member D-like) (Human mannose receptor) (hMR) (Macrophage mannose receptor 1-like protein 1) (CD antigen CD206)
OG0000058	– 8.122789399	Q8BN82	Sialin (H(+)/nitrate cotransporter) (H(+)/sialic acid cotransporter) (AST) (Solute carrier family 17 member 5) (Vesicular H(+)/Aspartate-glutamate cotransporter)
OG0000941	– 7.303135406	Q23490	Peroxidase mlt-7 (EC 1.11.1.7) (Molting defective protein 7) (MoLT-7) [Cleaved into: Peroxidase mlt-7 light chain; Peroxidase mlt-7 heavy chain]
OG0000082	– 7.3006886	Q9ET66,Q58D34	Peptidase inhibitor 16 (PI-16) (Cysteine-rich protease inhibitor) (CD antigen CD364),Peptidase inhibitor 16 (PI-16) (CD antigen CD364)
OG0000017	– 7.1921873	P03952	Plasma kallikrein (EC 3.4.21.34) (Fletcher factor) (Kininogenin) (Plasma prekallikrein) (PKK) [Cleaved into: Plasma kallikrein heavy chain; Plasma kallikrein light chain]
OG0000169	– 7.1508881	O42280,P43446	Protein Wnt-9a (Wnt-14),Protein Wnt-10a
OG0000130	– 7.0504759	Q66J54	Solute carrier family 22 member 6-A (Organic cation transporter 1-A) (Renal organic anion transporter 1-A) (ROAT1-A)
OG0000018	– 6.666119	XP_013083621.1	Uncharacterized protein
OG0000064	– 6.521116488	Q7TN88	Polycystic kidney disease protein 1-like 2 (PC1-like 2 protein) (Polycystin-1L2)
OG0000097	– 6.374237794	A0A6P8HC43	Actinia tenebrosa protease inhibitors (Carboxypeptidase inhibitor SmCI-like) [Cleaved into: ATPI-I; ATPI-II]
OG0000203	– 6.290408581	Q2LK54	Collectin-12 (Collectin-3) (CL-3) (cCL-3)
OG0005650	– 5.655833814	Q9HAU0	Pleckstrin homology domain-containing family A member 5 (PH domain-containing family A member 5) (Phosphoinositol 3-phosphate-binding protein 2) (PEPP-2)
OG0000067	– 5.475073679	Q20176	Zinc metalloproteinase nas-39 (EC 3.4.24.-) (Nematode astacin 39)
OG0000032	– 5.42187509	A0T2M3	Polcalcin Cup a 4 (Calcium-binding pollen allergen Cup a 4) (allergen Cup a 4)
OG0000049	– 5.183355035	P08537	Tubulin alpha chain [Cleaved into: Detyrosinated tubulin alpha chain]
OG0020149	– 5.054557451	P60204	Calmodulin (CaM)
OG0004334	– 4.949444349	P45961	Calexcitin-2
OG0000273	– 4.638245961	Q86YT5	Solute carrier family 13 member 5 (Na(+)/citrate cotransporter) (NaCT) (Sodium-coupled citrate transporter) (Sodium-dependent citrate transporter)
OG0000005	– 4.097023497	P04756	Acetylcholine receptor subunit alpha
OG0001594	– 3.811131228	Q7PCJ9	Thialysine N-epsilon-acetyltransferase (EC 2.3.1.-) (Diamine acetyltransferase 2) (EC 2.3.1.57) (Spermidine/spermine N(1)-acetyltransferase 2) (SSAT-2)
OG0001008	– 3.244828257	P82971	Phospholipase A2 (PLA2) (EC 3.1.1.4) (Phosphatidylcholine 2-acylhydrolase) (allergen Bom t 1)
OG0003351	– 3.097797925	XP_013087205.1	EF-hand domain-containing protein
OG0000137	– 3.000922693	Q499N5	Medium-chain acyl-CoA ligase ACSF2, mitochondrial (EC 6.2.1.2)

Also included are the Accession Number(s) of the best BLAST hits to NCBI and the associated protein annotation(s) from Goodheart et al. [41]. They are listed in the order of their log2FoldChange in *B. stephanieae*, meaning that Orthogroups closer to the top were more highly expressed in the Distal Ceras compared to the Proximal Ceras

Here, we hypothesize a few crucial steps for nematocyst sequestration, a modified version of phagocytosis, to evolve in nudibranchs, including a narrowing of function identified by a reduction in expression of many genes related to phagocytosis, immunity, and common digestive functions. Prior research in *B. stephanieae* found that putatively "novel" genes are not more commonly expressed in distal cerata compared to other, more conserved tissues such as the nervous system [41]. This finding suggests that nematocyst sequestration is likely a mix of subfunctionalization and neofunctionalization [50], where a more generalist phagocytic cell type, likely digestive cells, evolved for specificity to nematocyst uptake and storage using largely conserved processes [36, 41, 51]. Our results provide further support for this hypothesis, showing that a body region (i.e., the Distal Ceras with the cnidosac) with a novel function (i.e., nematocyst sequestration) appears to express many genes associated with phagocytosis, digestion, and immunity, but with lower expression than is found in other body regions with more generalized

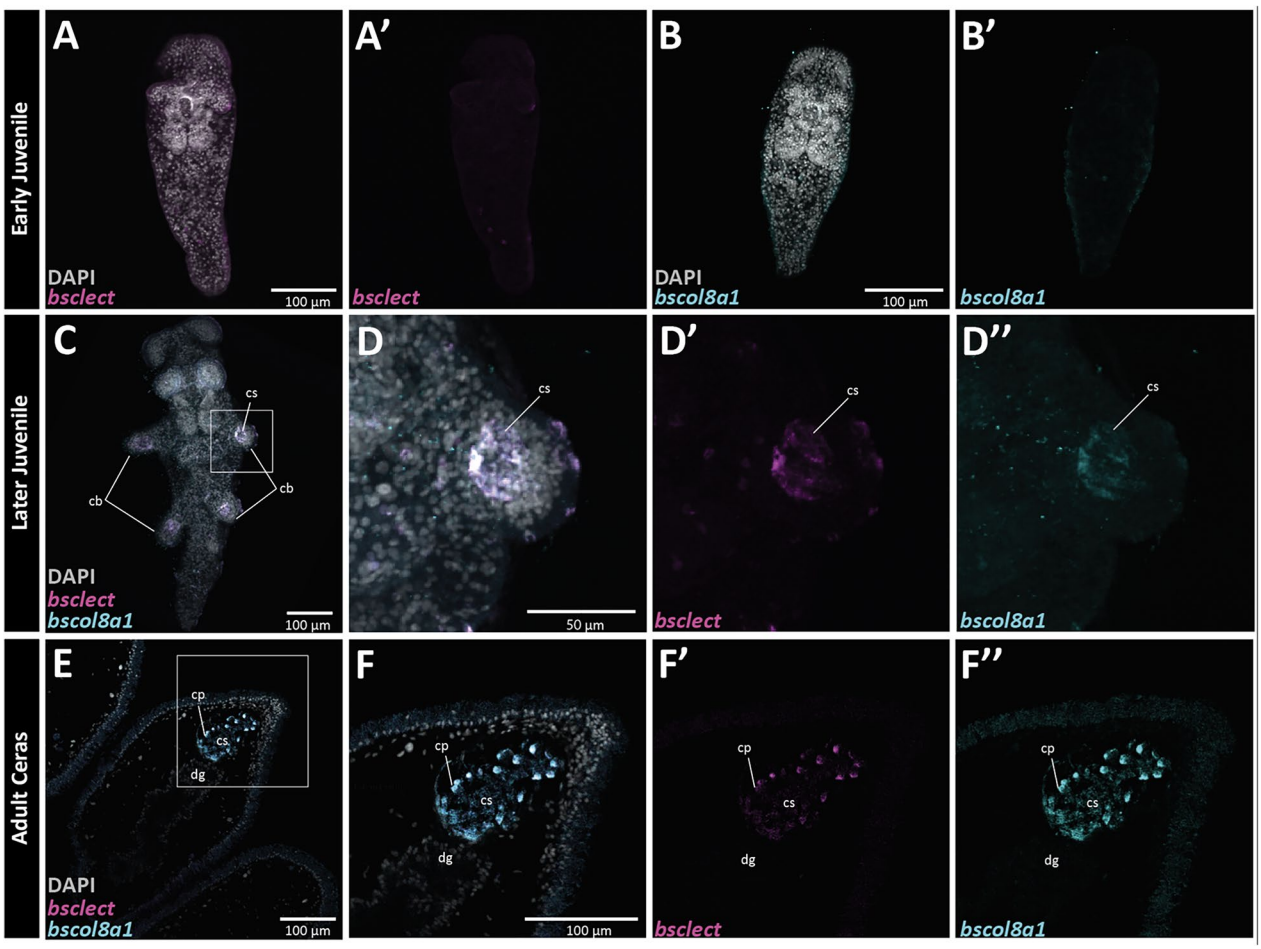

Fig. 3 Hybridization chain reaction (HCR) detected expression of cnidosac markers (*bsclect* and *bscola8a1*) during cerata development in *Berghia stephanieae*. Early juvenile expression of **A–A'** *bsclect* and **B–B'** *bscola8a1* prior to cerata development. Later juvenile co-expression of **C–D'''** *bsclect* and *bscola8a1* at the beginning of cerata development. Adult expression of **E–F'''** *bscola8a1* and *bsclect* in the ceras tissue. Abbreviated: cb, cerata buds; cs, cnidosac; cp, cnidophage; dg, digestive gland

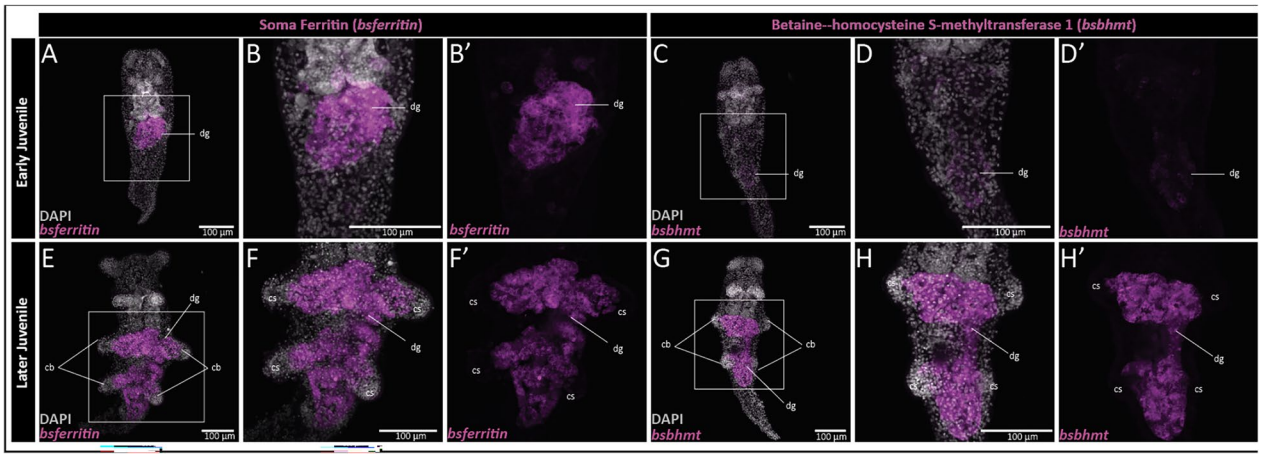

Fig. 4 Hybridization chain reaction (HCR) detected expression of digestive markers (*bsferritin* and *bsbhmt*) during cerata development in *Berghia stephanieae*. Early juvenile expression of (**A–B'**) *BsFerritin* and (**C–D'**) *bsbhmt* prior to cerata development. Later juvenile expression of (**E–F'**) *bsferritin* and (**G–H'**) *bsbhmt* at the beginning of cerata development. *cb* cerata buds, *cs* cnidosac, *cp* cnidophage, *dg* digestive gland

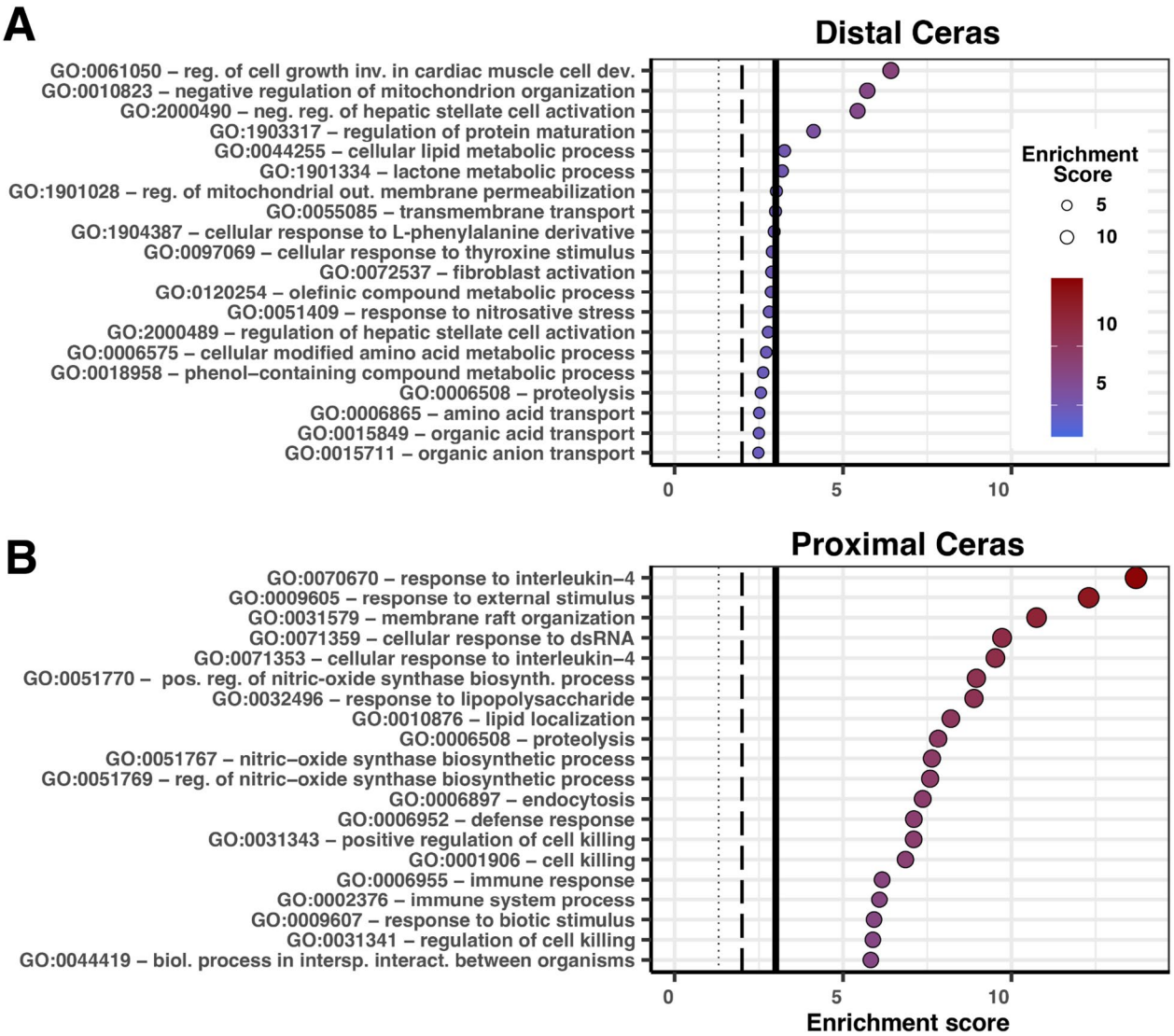

Fig. 5 Plots describing the most common GO terms associated with genes upregulated in the (**A**) distal and (**B**) proximal cerata in *B. stephanieae*. We used the Fisher statistic with the ParentChild algorithm to determine which terms were significantly upregulated. The enrichment score is the −log10() of the calculated p-value. The lines in the plot represent the enrichment score that aligns with significance values at: $p = 0.05$, small dotted line; $p = 0.01$, middle dashed line; and $p = 0.001$, thicker solid line. Enrichment scores are also represented in the size and color of the points, with larger and more red points representing lower *p*-values

phagocytic functions, like the Proximal Ceras (Figs. 5B, 6). We also show that nudibranch mollusks like *Berghia stephanieae* and *Hermissenda opalescens* offer opportunities for investigating how a conserved phenotype like phagocytosis results in a new phenotype like sequestration.

Distal cerata tissues have lower expression of digestion and immunity genes

Cerata in nudibranchs are made up of a number of tissue types, including neurosensory, epidermal, muscle, and digestive [14, 19]. Although the digestive gland and the cnidosac are only present in the proximal and distal cerata, respectively, many of the other functions of cerata are common to both tissue types. For example, cilial tufts are often distributed across the epidermis of the cerata, as are epidermal glandular cells [19], and hemocytes are often broadly distributed within the hemolymph (Fig. 1C). The functions of many of these glands remain unknown. It is unsurprising, therefore, that our results showed that the vast majority of genes expressed in the Proximal Ceras are also expressed in the Distal Ceras (87.3% overlap in *B stephanieae*). However, a clear separation in function exists between the proximal and distal cerata due to the presence of digestive gland tissue in the

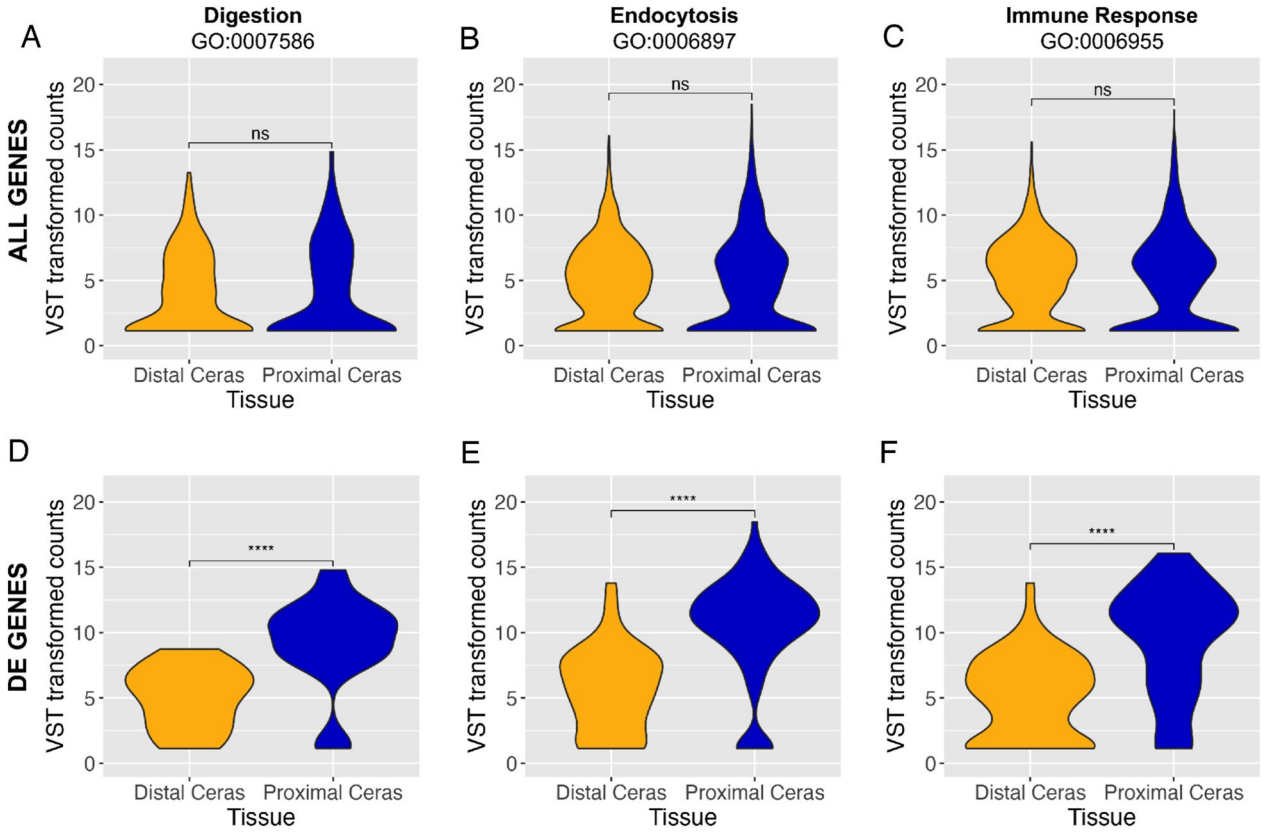

Fig. 6 Violin plots comparing VST transformed counts of genes in our analysis assigned particular GO terms: **A**, **D** GO:0007586, digestion (119 genes total; 9 DE genes); **B**, **E** GO:0006897, endocytosis (525 genes; 33 DE genes); **C**, **F** GO:0006955, immune response (838 genes; 52 DE genes). Plots are for subsets of genes associated with each of these three GO terms: **A**–**C** for all genes associated with each GO term, and **D**–**F** for only differentially expressed (DE) genes across both tissues associated with each GO term. Asterisks indicate level of significance between the two tissues (ns, $p > 0.05$; *$p \leq 0.05$; **$p \leq 0.01$; ***$p \leq 0.001$; ****$p \leq 0.0001$)

Proximal Ceras and the cnidosac in the Distal Ceras [14, 36, 52].

In the Proximal Ceras, the digestive gland is the primary internal tissue [14, 53]. In the digestive gland, at least two epithelial phagocytic cell types have been described, typically regarded as digestive and basophilic cells [54]. Digestive cells are the most abundant cell type in the digestive gland, and are characterized by an endocytic activity and intracellular digestion [54]. Basophilic cells, by contrast, are considered the primary cell type for secretion of enzymes for extracellular digestion. Our results are consistent with these reported functions. For example, we see downregulation of genes associated with digestion and immune function in the Distal Ceras (Figs. 5, 6; Table S6), with a higher expression of these genes in the Proximal Ceras compared to the Distal Ceras. We also identified some genes associated with digestion that are clearly only expressed in the digestive gland in *B. stephanieae*, including betaine–homocysteine S-methyltransferase (BHMT) and Soma Ferritin (Fig. 4), both of which are known to be used in mollusk digestion and metabolism [55, 56]. The expression of many of the other genes more highly expressed in the Proximal Ceras still needs to be examined via in situ hybridization methods to confirm exclusive expression in the digestive gland.

Distal cerata tissues have higher expression of select conserved genes

We hypothesized that cnidophages, the primary cell type of nematocyst sequestration, would have a narrower phagocytic function compared to digestive cells, where fewer phagocytosis, digestion, and or metabolism genes are expressed. Our results support the hypothesis that nematocyst sequestration likely represents—in part—a subfunctionalization of digestive processes. This subfunctionalization has resulted in only a small subset of metabolic, immunity, and endocytic genes more highly expressed in the Distal Ceras compared to the Proximal Ceras in both *B. stephanieae* and *H. opalescens*, including genes such as Cathepsin L, Snaclec, alpha-tubulin, and calmodulin (Table 1). Included in this list are Collagen

alpha-1(VIII) and macrophage mannose receptor 1, which we found are expressed exclusively within the cnidosac in both species (Fig. 3).

Many phagocytosis mechanisms are still crucial to the function of nematocyst sequestration, including receptors that target nematocysts and genes involved with engulfment and phagosome formation. We hypothesized that we would identify a complement of receptors in the cnidosac that may be specific to nematocysts and thus relate to the neofunctionalization of the cnidosac. We found in *B. stephanieae* that a subset of these putative phagocytic receptors more highly expressed in the Distal Ceras compared to the Proximal Ceras, including multiple C-type lectin macrophage mannose receptors, Sortilin-related receptors, and cation-dependent mannose-6-phosphate receptors (Table S8). Our results with *B. stephanieae* also showed that macrophage mannose receptor 1 (CLECT; Tables S3, S8) was the putative receptor with the highest expression in the Distal Ceras, and we found that it is co-expressed with Collagen alpha-1(VIII) exclusively in the cnidophages (Fig. 3). Our interpretation is further supported by morphological work showing that digestive gland cells do not appear to endocytose and digest nematocysts in most nudibranchs, as nematocysts have only rarely been found within digestive cells in aeolid nudibranchs [16] and then only at the very distal parts of the digestive gland [57]. The lack of nematocyst endocytosis in the digestive gland may be because nematocysts must be able to reach the cnidosac without being destroyed by digestive cells, and suggests that some level of neofunctionalization has to have occurred in the cnidosac. However, previous work in Hancockiidae nudibranchs, a group representing a second origin of nematocyst sequestration in nudibranchs, has shown that nematocysts are endocytosed within the digestive gland in addition to the cnidosac. This difference between aeolids and dendronotid nudibranchs [51] provides an important distinction that would allow us to further test this hypothesis.

Outside of their need for target specificity, cnidophages still need to perform other conserved phagocytosis functions, such as the engulfment of the material and phagosome formation, which requires the conserved actin–myosin contractile system [58] and the microtubule system [57]. We found alpha-tubulin upregulated in both *B. stephanieae* and *H. opalescens* (Table 1) and both actin and myosin upregulated in the Distal Ceras in *B. stephanieae* (Table S3), which is in agreement with our assertion. However, it is possible that some of these genes produce different protein isoforms that have different functions between the two tissues [59], which would not be detectable in our analysis. Finally, we cannot yet reject the hypothesis that cnidophages are not the source of this difference; further analysis comparing expression profiles of cnidophage cells with that of other phagocytes (using techniques such as single-cell RNA-seq) are still necessary.

The role of conserved genes in nematocyst sequestration

The role of conserved genes in nematocyst sequestration is still not fully resolved, but our data suggest that conserved genes are likely critical to the novel function of nematocyst sequestration in cnidophages. In other systems where cells or structures are engulfed and stored intracellularly, such as cnidarian–dinoflagellate endosymbiosis, squid–Vibrio symbiosis, plant–microbe symbiosis, and insect–bacterial symbiosis, it is clear that many metazoan cells use pattern recognition receptors (PRRs) to identify pathogen-associated molecular patterns (PAMPs) like peptidoglycans and lipopolysaccharides [28–31]. We found PRRs, and particularly mannose receptors, expressed in the Distal Ceras of both nudibranch species (Table S8), and expressed exclusively within the cnidophages of *B. stephanieae* (Fig. 5), which supports this hypothesis. Mollusks have also undergone a large-scale expansion and molecular divergence of PRRs and signaling adapters, as well as significant recombination of immune receptors and fibrinogen-related proteins FREPs [60]. This may be part of the reason that mollusks like nudibranchs have evolved multiple types of phagocytic specializations, including nematocyst sequestration [52], kleptoplasty [61], and endosymbioses [62, 63].

However, some of these conserved genes may not necessarily retain precisely the same functions across phagocytic tissues and across large phylogenetic distances. For example, evidence suggests that in cnidarian–dinoflagellate endosymbiosis, activation of the host transforming growth factor beta (TGFβ) innate immune pathway actually promotes tolerance of the symbiont rather than destruction [64]. This is consistent with the function of TGFβ immune regulation in mammals, as this pathway plays an important role in maintaining peripheral tolerance against self- and innocuous antigens [65]. We, and others [66], have found no evidence to support the role of the TFGβ pathway in maintenance of sequestered nematocysts or symbionts in *B. stephanieae* or *H. opalescens*. It is clear that conserved genes are important in the evolution of novelties like sequestration and endosymbiosis, but the mechanisms driving the recruitment and co-option of certain genes and pathways are complex, and may be different in systems where specific organelles are the primary targets.

Conclusions

Nematocyst sequestration, a process by which stinging organelles from cnidarians are stolen and stored intracellularly, is a novel function that relies on highly conserved phagocytic functions. As such, it is an excellent system in which to investigate how conserved functions can be modified to produce novel phenotypes. Our results clearly indicate that Distal Ceras tissues have very high expression of certain genes known to be associated with phagocytosis, including at least one that may be used for targeting nematocysts that we found expressed in the cnidophage cells. We also found that sequestering tissues tend to have lower expression of genes associated with digestion compared to digestive tissues. Although the role of conserved genes in nematocyst sequestration is still not fully resolved, our data suggest that many are critical to nematocyst sequestration despite the novel nature of this physiological process. From these results, we hypothesize a more detailed model for the evolution of the molecular mechanism of nematocyst sequestration, including: (1) the evolution of a means of specificity for targeting nematocysts over other tissues and structures; (2) modifications to internalization and phagosome formation pathways to accommodate multiple large and unusually shaped objects; and (3) the loss of some functions related to phagosome maturation, immunity, and common metabolic functions. This study lays the foundation for further inquiry into mechanisms of organelle sequestration in nudibranchs and other organisms.

Methods

Specimen collection

Hermissenda opalescens were collected from the wild at the Monterey Municipal Wharf #2 (36.60398, − 121.88898) on 4 April 2019 and 14 September 2019 under permit SC-3726 from the State of California Department of Fish and Wildlife to TJH.

We maintained adults of *Berghia stephanieae* in continuous culture in the Lyons Lab at the Scripps Institution of Oceanography (SIO) or the Goodheart Lab at the American Museum of Natural History (AMNH), broadly following techniques laid out by Goodheart et al. [36, 41]. We purchased original *Berghia stephanieae* animals for from the company ReefTown (https://reeftown.com). We fed *B. stephanieae* maintained in the lab with the anemone *Exaiptasia diaphana*. At SIO, we purchased *E. diaphana* from Carolina Biological Supply, Burlington, NC; at AMNH we purchased *E. diaphana* from the Marine Biological Laboratory, Woods Hole, MA.

Transcriptomic data analysis

We obtained *Berghia stephanieae* Distal (3 samples; SRR12072207, SRR25598596-SRR25598597) and Proximal Ceras (3 samples; SRR12072208, SRR25598594-SRR25598595) read mapping data from the previously published *B. stephanieae* genome paper [41] through NCBI. To collect Proximal and Distal Ceras samples for *B. stephanieae*, we removed cerata and separated the region with the cnidosac (Distal Ceras) from the region with the digestive gland (Proximal Ceras) at the narrow entrance to the cnidosac (Fig. 1C) [14].

Transcriptome data for *H. opalescens* (SRR32330727-SRR32330757) were obtained from an experiment in which cerata were removed from field-collected animals and allowed to regrow. During the regrowth period, nudibranchs were separated into two experimental groups and maintained at 14 °C in separate chambers. One group was fed daily with *Aurelia aurita* (moon jelly) polyps ("N"); the other was fed a non-nematocyst food source such as mussel, squid, or tunicate ("C"). Once the cerata were regrown (30–40 days later, [67]), we removed all cerata from the right side of the body and sectioned each into three parts: (1) the cnidosac ("Distal Ceras"); (2) "cer," the region from between the cnidosac to about 2/3 the distance towards the body of the animal; and (3) "sub" ("Proximal Ceras"), the remaining region closest to the body of the animal. At this time, we also sampled foot tissue (i.e., not within the cerata) from each nudibranch. Total RNA was extracted from 5–10 pooled cerata tissues (separated by individual and section type) using TRIzol (Life Technologies), and mRNA was reverse transcribed using NEXTflexTM Poly(A) Beads (Bioo Scientific) and SuperScript® III Reverse Transcriptase (Life Technologies). The resulting cDNA was made into libraries using the NEXTflex Directional RNAseq Kit and sent for two lanes of 2×150 paired-end sequencing on the Illumina HiSeq4000 at QB3 Genomics (UC Berkeley, Berkeley, CA, RRID:SCR_022170).

For reference transcriptomes, we used the unfiltered BRAKER2 gene prediction (59,494 genes, 61,662 proteins) in the published *Berghia stephanieae* genome paper [41] as our *B. stephanieae* reference, and downloaded *Hermissenda opalescens* transcriptome data from NCBI (SRR1950939, [34]) to build our *H. opalescens* reference transcriptome. The *H. opalescens* reference transcriptome was generated using the protocol laid out in Goodheart et al. [41]. Briefly, using the previously assembled version of the *H. opalescens* transcriptome [68], we predicted open reading frames (ORFs) with TransDecoder (version 5.5.0 [69]) and clustered predicted ORFs using CD-HIT-EST (version 4.8.1 [70, 71]) at 95% identity and word size of 11 (-c 0.95, -n 11). Post-clustering, we filtered transcripts with alien_index (https://github.com/josephryan/alien_index); based on an algorithm described [72]). We removed all sequences with an alien index greater than 45 from the transcriptome. We then compiled full transcripts for each predicted ORF

sequence remaining from the assembled transcriptome using a custom Python script (full_transcripts.py, [41]).

We mapped reads to the *B. stephanieae* genome using STAR v2.7.9a [73] with default parameters plus additional flags (–readFilesCommand zcat –outSAMtype BAM SortedByCoordinate –twopassMode Basic –sjdbGTFfeatureExon 'CDS'). We mapped reads to the *H. opalescens* reference transcriptome using Bowtie 2 v.2.4.4 [74]. We counted reads using the command htseq-count from the HTSeq framework v1.99.2 [75]. We analyzed counts using the DESeq function from DESeq2 v1.26.0 [76] to perform differential expression analysis, and generated the results using the results function. DESeq2 uses the median of ratios approach to normalize the counts data taking into account sequencing depth and RNA composition. We considered genes upregulated if the adjusted p-value (padj) was less than 0.05 and log2FoldChange was greater than 2. Genes were considered exclusively expressed in a certain tissue if the average number of reads across all samples was > 0.5 in that tissue and < 0.5 in the other, which would mean that gene had a count of 1 in at least two samples. Orthology of *B. stephanieae* genes to *H. opalescens* transcripts was assigned using output from the OrthoFinder [77, 78] analysis in Goodheart et al. [41].

Putative gene function was assigned based on GO terms. To assess which GO terms were significantly enriched in our two tissues, we used the Fisher's Exact test implemented in the R package TopGO [79]. To directly compare expression of genes that fall under particular GO terms (Table S7), we performed a paired t-test implemented in ggpubr [80] that compared variance-stabilizing transformation (VST) counts (transformation performed on DESeq2 normalized counts) from the same gene between Proximal and Distal Cerata. VST transformation counts were used to make the data homoskedastic, and VST was selected because the range of size factors was < 4 [76]. These comparisons were used to evaluate whether genes associated with certain GO terms were more likely to be highly expressed in one set of tissues over another, particularly those that were considered differentially expressed.

Tissue fixation and paraffin section preparation

We cultured and relaxed *B. stephanieae* juveniles using the same methods from prior *B. stephanieae* imaging work [36, 41, 81]. Prior to fixation, we starved juveniles for 3 days. Post-relaxation, we fixed juveniles using 4% paraformaldehyde (PFA, diluted in filtered sea water from 16% ampules). We washed samples in a 50% 1× PBS/50% methanol solution for 10 min prior to three washes in 100% methanol for 10 min, all at room temperature. We stored samples in 100% methanol at – 20 °C for up to 3 months prior to HCR experiments. For adult *B. stephanieae*, we incubated individuals at 4C until fully relaxed and then fixed adults with a 4% PFA (diluted in DEPC-treated 1× PBS) incubation overnight at 4 °C. We washed and stored samples following the same protocol described for juveniles. Fixed samples that were put into paraffin immediately were dehydrated into 75% ethanol instead of 100% methanol.

To prepare fixed adult *B. stephanieae* for paraffin wax embedding (paraplast wax), we first placed the samples into 100% ethanol with two 100% ethanol washes for 2 min. We cleared the samples with three 20-min washes in Histosol on a shaker at room temperature. We then washed samples in 50% Histosol 50% paraffin wax twice for 30 min each at 60 °C. We left the samples in 100% paraffin wax overnight at 60 °C, and then performed four 1-h paraffin washes at 60 °C before embedding the sample in paraffin using a mold. We sectioned samples using a Leica Biosystems RM2245 microtome to a thickness of 10 µM. We floated sectioned samples in water before mounting onto Fisherbrand™ Superfrost™ Plus slides (FisherScientific #22-037-246). We then incubated the samples at 37 °C overnight before storing them at room temperature until further use.

Hybridization chain reaction

We designed all HCR probe sets using the HCR 3.0 probe maker with either the B1 or B2 amplifier (ÖzpolatLab-HCR, 2021, Kuehn et al.) for up to 30 probe pairs (Tables S9–S13). We ordered probe sets (50 pmol DNA oPools Oligo Pool) from Integrated DNA Technologies (Coralville, IA), which we resuspended to 1 pmol/µL in 50 mL TE buffer or RNase-free ultrapure water and RNA and stored at – 20 °C.

For whole-mount juvenile HCR, we used a modified HCR 3.0 protocol for *Berghia stephanieae* using the same solution recipes from Choi et al. [43] and modifications according to Goodheart et al. [41]. Following the Hoechst staining, we mounted samples in a 20% 5× SSCT, 80% glycerol solution and we followed the imaging process described in Goodheart et al. [41]. For HCR on paraffin sections, we followed the protocol from Choi et al. [43] with the modifications described in Criswell and Gillis [82]. We used the same probe and amplifier concentrations described in Goodheart et al. [41] for both whole-mount and paraffin section HCR.

Fluorescent imaging

We imaged whole-mount and paraffin-sectioned HCR samples with a Zeiss LSM 710 inverted confocal microscopes located at SIO and AMNH, respectively. We analyzed and processed images with software ImageJ FIJI

and AdobePhotoshop [83] (Adobe Inc., California, USA). We stitched images together using the FIJI Pairwise Stitching Plugin [84]. We created figures in Adobe Illustrator (Adobe Inc., California, USA).

Abbreviation
HCR Hybridization chain reaction

Supplementary Information

The online version contains supplementary material available at https://doi.org/10.1186/s13227-025-00241-x.

Supplementary Material 1.
Supplementary Material 2.
Supplementary Material 3.
Supplementary Material 4.
Supplementary Material 5.
Supplementary Material 6.
Supplementary Material 7.
Supplementary Material 8.
Supplementary Material 9.
Supplementary Material 10.
Supplementary Material 11.
Supplementary Material 12.
Supplementary Material 13.
Supplementary Material 14.

Acknowledgements
We thank all members of the Goodheart, Lyons, and Katz labs for help with animal care and feedback on this project and manuscript, particularly M. Desmond Ramirez, who was instrumental in helping us establish HCR in juveniles. We thank the Holford and Gillis labs for helping us establish paraffin section HCR in B. Stephanieae. We are also grateful to members of the Berghia Brain Project (https://sites.google.com/umass.edu/berghiabrainproject/) for their feedback on this project. We also thank the Hamdoun Lab and the AMNH Microscopy Imaging Facility for the use of their confocal microscopes, the Rouse Lab for the use of their Qubit, and the AMNH Institute for Comparative Genomics for assistance with the laboratory portion of this work. We also thank Connor Tumelty, Yin Chen Wan, Kristen Tamsil, and Kate Montana for assistance with *H. opalescens* care, Dr. Freeland Dunker, Kylie Lev, and other staff at the California Academy of Sciences for donating moon jelly polyps to the project, and Lydia Smith and the Evolutionary Genetics Lab for assistance with RNA extractions and library preparations. We are also grateful for the work of the editor and reviewers of our manuscript. This work is in memory of our outstanding colleague Dr. Maryna P. Lesoway, who provided significant intellectual and emotional support in executing this work.

Author contributions
JAG, NM, TDT, and DCL conceived of the study; JAG, RAF, RDT, NM, TJH, and RLA collected data; JAG, RDT, and RAR performed data analyses; all authors contributed to study design, participated in data interpretation, and read and approved the final manuscript.

Funding
This work was supported by a Scripps Postdoctoral Fellowship and startup from the AMNH to JAG, and NIH BRAIN awards U01-NS108637 and 1U01-NS123972, an Emerging Research Organisms Grant from the Society for Developmental Biology to DCL, start-up funding from UC Berkeley to RDT, and a 2019 Conchologists of America Academic Grant to NM. RDT is also supported by NIH NIGMS R35GM150574. This work also used the Extreme Science and Engineering Discovery Environment (XSEDE) at the San Diego Supercomputer Center (SDSC) through allocation IDs TG-BIO210019 and TG-BIO210138 [85], which is supported by National Science Foundation grant number ACI-1548562, as well as the Savio computational cluster resource provided by the Berkeley Research Computing program at the University of California, Berkeley (supported by the UC Berkeley Chancellor, Vice Chancellor for Research, and Chief Information Officer). Sequencing at QB3 Genomics on the Illumina HiSeq 4000 platform was supported by NIH S10 OD018174 Instrumentation Grant.

Availability of data and materials
Raw sequencing data used are accessible through the NCBI Sequence Read Archive (BioProjects PRJNA1004233, PRJNA641185, and PRJNA1222994), including for the Distal (3 samples; SRR12072207, SRR25598596-SRR25598597) and Proximal Ceras (3 samples; SRR12072208, SRR25598594-SRR25598595) samples for Berghia stephanieae and samples from multiple tissue types in Hermissenda opalescens. The genome used is available at DDBJ/ENA/GenBank under the accession JAWQJI000000000. Input and intermediate files for our analyses are available in Dryad (https://doi.org/10.5061/dryad.8pk0p2p00) and custom R scripts used in our analyses are available through Github (https://github.com/goodgodric28/sequestration_genes/tree/main/sequestration_genes).

Declarations

Ethics approval and consent to participate
Not applicable.

Consent for publication
Not applicable.

Competing interests
The authors declare that they have no competing interests.

Author details
[1]Division of Invertebrate Zoology, American Museum of Natural History, New York, NY, USA. [2]Scripps Institution of Oceanography, University of California, San Diego, La Jolla, CA, USA. [3]Department of Integrative Biology, University of California, Berkeley, CA, USA. [4]Museum of Vertebrate Zoology, University of California, Berkeley, CA, USA. [5]Present Address: Marine Biological Laboratory, Woods Hole, MA, USA. [6]Richard Gilder Graduate School, American Museum of Natural History, New York, NY, USA.

Received: 17 February 2025 Accepted: 19 April 2025
Published online: 28 June 2025

References

1. Mills DB. The origin of phagocytosis in Earth history. Interface Focus. 2020;10:20200019.
2. Jain N, Moeller J, Vogel V. Mechanobiology of macrophages: how physical factors coregulate macrophage plasticity and phagocytosis. Annu Rev Biomed Eng. 2019;21:267–97.
3. Niedergang F. Phagocytosis. In: Encyclopedia of cell biology. Amsterdam: Elsevier; 2016. p. 751–7. https://doi.org/10.1016/b978-0-12-394447-4.20073-4.
4. Applequist SE, Wallin RPA, Ljunggren H-G. Variable expression of Toll-like receptor in murine innate and adaptive immune cell lines. Int Immunol. 2002;14:1065–74.
5. Bundscherer L, Wende K, Ottmüller K, Barton A, Schmidt A, Bekeschus S, et al. Impact of non-thermal plasma treatment on MAPK signaling pathways of human immune cell lines. Immunobiology. 2013;218:1248–55.
6. Nakamura T, Kuroi M, Fujiwara Y, Warashina S, Sato Y, Harashima H. Small-sized, stable lipid nanoparticle for the efficient delivery of siRNA to human immune cell lines. Sci Rep. 2016;6:37849.
7. Lu X-J, Deng Q, Thompson KD. Editorial: the function of phagocytes in non-mammals. Front Immunol. 2020;11: 628847.
8. Gold KS, Brückner K. Macrophages and cellular immunity in Drosophila melanogaster. Semin Immunol. 2015;27:357–68.

9. Reddien PW, Cameron S, Horvitz HR. Phagocytosis promotes programmed cell death in *C. elegans*. Nature. 2001;412:198–202.
10. Mao Y, Finnemann SC. Regulation of phagocytosis by Rho GTPases. Small GTPases. 2015;6:89–99.
11. Anderson OR. Intracellular digestion. Am Biol Teach. 1970;32:461–7.
12. Goodheart JA, Bely AE. Sequestration of nematocysts by divergent cnidarian predators: mechanism, function, and evolution. Invertebr Biol. 2017. https://doi.org/10.1111/ivb.12154.
13. Greenwood PG. Acquisition and use of nematocysts by cnidarian predators. Toxicon. 2009;54:1065–70.
14. Goodheart JA, Bleidißel S, Schillo D, Strong EE, Ayres DL, Preisfeld A, et al. Comparative morphology and evolution of the cnidosac in Cladobranchia (Gastropoda: Heterobranchia: Nudibranchia). Front Zool. 2018;15:43.
15. Ohkawa K, Yamasu T. The stored nematocysts in aeolid nudibranchs. Report of the Fukaura Marine Biological Laboratory, Hirosaki University. 1993; pp. 17–24.
16. Yamamoto G, Kanai N, Miura T, Oguchi K. Blue angels have devil hands: predatory behavior using cerata in *Glaucus atlanticus*. Ecology. 2025;106: e70062.
17. Delgado V, Barrios EE, Bujanda A, Araque W. Surface morphology and characteristics of hemocytes of *Biomphalaria glabrata* (Pulmonata: Planorbidae) from two geographic sources. Rev Latinoam Microbiol. 2001;43:114–8.
18. Aguado F, Marin A. Warning coloration associated with nematocyst-based defences in aeolidiodean nudibranchs. J Molluscan Stud. 2007;73:23–8. https://doi.org/10.1093/mollus/eyl026.
19. Edmunds M. Protective mechanisms in the Eolidacea (Mollusca Nudibranchia). J Linnean Soc Lond Zool. 1966;46:27–71. https://doi.org/10.1111/j.1096-3642.1966.tb00082.x.
20. Stachowicz JJ, Lindquist N. Hydroid defenses against predators: the importance of secondary metabolites versus nematocysts. Oecologia. 2000;124:280–8.
21. Bullard SG, Hay ME. Palatability of marine macro-holoplankton: nematocysts, nutritional quality, and chemistry as defenses against consumers. Limnol Oceanogr. 2002;47:1456–67. https://doi.org/10.4319/lo.2002.47.5.1456.
22. Le Guernic A, Geffard A, Le Foll F, Palos LM. Comparison of viability and phagocytic responses of hemocytes withdrawn from the bivalves *Mytilus edulis* and *Dreissena polymorpha*, and exposed to human parasitic protozoa. Int J Parasitol. 2020;50:75–83.
23. Yang W, Lv X, Leng J, Li Y, Sun J, Yang C, et al. A fibrinogen-related protein mediates the recognition of various bacteria and haemocyte phagocytosis in oyster *Crassostrea gigas*. Fish Shellfish Immunol. 2021;114:161. https://doi.org/10.1016/j.fsi.2021.04.022.
24. Huang Q, Yu M, Chen H, Zeng M, Sun Y, Saha TT, et al. LRFN (leucine-rich repeat and fibronectin type-III domain-containing protein) recognizes bacteria and promotes hemocytic phagocytosis in the Pacific oyster *Crassostrea gigas*. Fish Shellfish Immunol. 2018;72:622–8. https://doi.org/10.1016/j.fsi.2017.11.049.
25. Gagnaire B, Frouin H, Moreau K, Thomas-Guyon H, Renault T. Effects of temperature and salinity on haemocyte activities of the Pacific oyster, *Crassostrea gigas* (Thunberg). Fish Shellfish Immunol. 2006;20:536–47. https://doi.org/10.1016/j.fsi.2005.07.003.
26. Itoh N, Takahashi KG. A novel peptidoglycan recognition protein containing a goose-type lysozyme domain from the Pacific oyster, *Crassostrea gigas*. Mol Immunol. 2009;46:1768–74. https://doi.org/10.1016/j.molimm.2009.01.022.
27. Schoenberg DA, Cheng TC. Lectin-binding specificities of hemocytes from two strains of *Biomphalaria glabrata* as determined by microhemadsorption assays. Dev Comp Immunol. 1980;4:617–28.
28. Collins AJ, Schleicher TR, Rader BA, Nyholm SV. Understanding the role of host hemocytes in a squid/vibrio symbiosis using transcriptomics and proteomics. Front Immunol. 2012;3:91.
29. Davy SK, Allemand D, Weis VM. Cell biology of cnidarian-dinoflagellate symbiosis. Microbiol Mol Biol Rev. 2012;76:229–61.
30. Saijo Y, Loo EP-I, Yasuda S. Pattern recognition receptors and signaling in plant–microbe interactions. Plant J. 2018;93:592–613.
31. Harris HL, Brennan LJ, Keddie BA, Braig HR. Bacterial symbionts in insects: balancing life and death. Symbiosis. 2010;51:37–53.
32. Valdés A. A new species of *Aeolidiella* Bergh, 1867 (Mollusca: Nudibranchia: Aeolidiidae) from the Florida keys, USA. Veliger. 2005;47:218–23.
33. Goodheart JA, Bazinet AL, Valdés Á, Collins AG, Cummings MP. Prey preference follows phylogeny: evolutionary dietary patterns within the marine gastropod group Cladobranchia (Gastropoda: Heterobranchia: Nudibranchia). BMC Evol Biol. 2017;17:221.
34. Goodheart JA, Bazinet AL, Collins AG, Cummings MP. Relationships within Cladobranchia (Gastropoda: Nudibranchia) based on RNA-Seq data: an initial investigation. R Soc Open Sci. 2015;2: 150196.
35. Karmeinski D, Meusemann K, Goodheart JA, Schroedl M, Martynov A, Korshunova T, et al. Transcriptomics provides a robust framework for the relationships of the major clades of cladobranch sea slugs (Mollusca, Gastropoda, Heterobranchia), but fails to resolve the position of the enigmatic genus *Embletonia*. BMC Ecol Evol. 2021;21:226.
36. Goodheart JA, Barone V, Lyons DC. Movement and storage of nematocysts across development in the nudibranch *Berghia stephanieae* (Valdés, 2005). Front Zool. 2022;19:16.
37. Lindsay T, Valdés Á. The model organism *Hermissenda crassicornis* (Gastropoda: Heterobranchia) is a species complex. PLoS ONE. 2016;11: e0154265.
38. Uribe-Querol E, Rosales C. Phagocytosis: our current understanding of a universal biological process. Front Immunol. 2020;11:1066.
39. Rosales C, Uribe-Querol E. Phagocytosis: a fundamental process in immunity. BioMed Res Int. 2017;2017:1–18. https://doi.org/10.1155/2017/9042851.
40. Günther J, Seyfert H-M. The first line of defence: insights into mechanisms and relevance of phagocytosis in epithelial cells. Semin Immunopathol. 2018;40:555–65.
41. Goodheart JA, Rio RA, Taraporevala NF, Fiorenza RA, Barnes SR, Morrill K, et al. A chromosome-level genome for the nudibranch gastropod *Berghia stephanieae* helps parse clade-specific gene expression in novel and conserved phenotypes. BMC Biol. 2024;22:9.
42. Law CW, Alhamdoosh M, Su S, Dong X, Tian L, Smyth GK, et al. RNA-seq analysis is easy as 1–2–3 with limma, Glimma and edgeR. F1000Research. 2016;5:1408. https://doi.org/10.12688/f1000research.9005.3.
43. Choi HMT, Schwarzkopf M, Fornace ME, Acharya A, Artavanis G, Stegmaier J, et al. Third-generation hybridization chain reaction: multiplexed, quantitative, sensitive, versatile, robust. Development. 2018. https://doi.org/10.1242/dev.165753.
44. Huan P, Liu G, Wang H, Liu B. Multiple ferritin subunit genes of the Pacific oyster *Crassostrea gigas* and their distinct expression patterns during early development. Gene. 2014;546:80–8.
45. Zhang Y, Sun J, Mu H, Li J, Zhang Y, Xu F, et al. Proteomic basis of stress responses in the gills of the pacific oyster *Crassostrea gigas*. J Proteome Res. 2015;14:304–17.
46. Phagocytosis GS. An immunobiologic process. Immunity. 2016;44:463–75.
47. Adema CM, Bayne CJ, Bridger JM, Knight M, Loker ES, Yoshino TP, et al. Will all scientists working on snails and the diseases they transmit please stand up? PLoS Negl Trop Dis. 2012;6: e1835.
48. Abrams TW. Studies on *Aplysia* neurons suggest treatments for chronic human disorders. Curr Biol. 2012;22:R705–11.
49. Davison A, Neiman M. Mobilizing molluscan models and genomes in biology. Philos Trans R Soc Lond B Biol Sci. 2021;376:20200163.
50. Pomaville MB, Sattler SM, Abitua PB. A new dawn for the study of cell type evolution. Development. 2024;151. https://doi.org/10.1242/dev.200884.
51. Martin R, Heß M, Schrödl M, Tomaschko K-H. Cnidosac morphology in dendronotacean and aeolidacean nudibranch molluscs: from expulsion of nematocysts to use in defense? Mar Biol. 2009;156:261–8.
52. Goodheart JA, Bely AE. Sequestration of nematocysts by divergent cnidarian predators: mechanism, function, and evolution. Invertebr Biol. 2017;136:75–91.
53. Moles J, Wägele H, Ballesteros M, Pujals Á, Uhl G, Avila C. The end of the cold loneliness: 3D comparison between *Doto antarctica* and a new sympatric species of *Doto* (heterobranchia: Nudibranchia). PLoS ONE. 2016;11: e0157941.
54. Lobo-da-Cunha A. Structure and function of the digestive system in molluscs. Cell Tissue Res. 2019;377:475–503.

55. Weis JS. Feeding and digestion. In: Physiological developmental and behavioral effects of marine pollution. Springer, Netherlands: Dordrecht; 2014. p. 37–64.
56. Habib MR, Bu L, Posavi M, Zhong D, Yan G, Zhang S-M. Yolk proteins of the schistosomiasis vector snail *Biomphalaria glabrata* revealed by multi-omics analysis. Sci Rep. 2024;14:1820.
57. Harrison RE, Grinstein S. Phagocytosis and the microtubule cytoskeleton. Biochem Cell Biol. 2002;80:509–15.
58. Barger SR, Gauthier NC, Krendel M. Squeezing in a meal: myosin functions in phagocytosis. Trends Cell Biol. 2020;30:157–67.
59. Bhuiyan SA, Ly S, Phan M, Huntington B, Hogan E, Liu CC, et al. Systematic evaluation of isoform function in literature reports of alternative splicing. BMC Genomics. 2018;19:637.
60. Li Y, Xue Y, Peng Z, Zhang L. Immune diversity in lophotrochozoans, with a focus on recognition and effector systems. Comput Struct Biotechnol J. 2023;21:2262–75.
61. Händeler K, Grzymbowski YP, Krug PJ, Wägele H. Functional chloroplasts in metazoan cells—a unique evolutionary strategy in animal life. Front Zool. 2009;6:28.
62. Rola M, Frankenbach S, Bleidissel S, Sickinger C, Donath A, Frommlet JC, et al. Cladobranchia (Gastropoda, Nudibranchia) as a promising model to understand the molecular evolution of photosymbiosis in animals. Front Mar Sci. 2022. https://doi.org/10.3389/fmars.2021.745644.
63. Pang CZ, Boo MV, Ip YK, Chew SF. Symbiotic dinoflagellates of the giant clam, *Tridacna squamosa*, express ammonium transporter 2 at the plasma membrane and increase its expression levels during illumination. Front Mar Sci. 2022. https://doi.org/10.3389/fmars.2022.835574.
64. Detournay O, Schnitzler CE, Poole A, Weis VM. Regulation of cnidarian-dinoflagellate mutualisms: evidence that activation of a host TGFβ innate immune pathway promotes tolerance of the symbiont. Dev Comp Immunol. 2012;38:525–37.
65. Sanjabi S, Oh SA, Li MO. Regulation of the immune response by TGF-β: from conception to autoimmunity and infection. Cold Spring Harb Perspect Biol. 2017;9: a022236. https://doi.org/10.1101/cshperspect.a022236.
66. Clavijo JM, Sickinger C, Bleidißel S, Gasparoni G, Tierling S, Preisfeld A, et al. The nudibranch *Berghia stephanieae* (Valdés, 2005) is not able to initiate a functional symbiosome-like environment to maintain *Breviolum minutum* (J.E. Parkinson & LaJeunesse 2018). Front Mar Sci. 2005. https://doi.org/10.3389/fmars.2022.934307.
67. Miller JA, Byrne M. Ceratal autotomy and regeneration in the aeolid nudibranch *Phidiana crassicornis* and the role of predators. Invertebr Biol. 2000;119:167–76.
68. Goodheart JA, Wägele H. Phylogenomic analysis and morphological data suggest left-right swimming behavior evolved prior to the origin of the pelagic Phylliroidae (Gastropoda: Nudibranchia). Org Divers Evol. 2020;20:657–67.
69. Haas BJ. TransDecoder. 2018. Available from: https://github.com/TransDecoder/TransDecoder.
70. Li W, Godzik A. Cd-hit: a fast program for clustering and comparing large sets of protein or nucleotide sequences. Bioinformatics. 2006;22:1658–9.
71. Fu L, Niu B, Zhu Z, Wu S, Li W. CD-HIT: accelerated for clustering the next-generation sequencing data. Bioinformatics. 2012;28:3150–2.
72. Ryan JF. Alien_index: Alien_index first release [Internet]. Zenodo; 2015.https://doi.org/10.5281/ZENODO.21029.
73. Dobin A, Davis CA, Schlesinger F, Drenkow J, Zaleski C, Jha S, et al. STAR: ultrafast universal RNA-seq aligner. Bioinformatics. 2013;29:15–21.
74. Langmead B, Salzberg SL. Fast gapped-read alignment with Bowtie 2. Nat Methods. 2012;9:357–9.
75. Putri GH, Anders S, Pyl PT, Pimanda JE, Zanini F. Analysing high-throughput sequencing data in Python with HTSeq 2.0. arXiv [q-bio.GN]. 2021. Available from: http://arxiv.org/abs/2112.00939.
76. Love MI, Huber W, Anders S. Moderated estimation of fold change and dispersion for RNA-seq data with DESeq2. Genome Biol. 2014;15:550.
77. Emms DM, Kelly S. OrthoFinder: phylogenetic orthology inference for comparative genomics. Genome Biol. 2019;20:238.
78. Emms DM, Kelly S. OrthoFinder: solving fundamental biases in whole genome comparisons dramatically improves orthogroup inference accuracy. Genome Biol. 2015;16:157.
79. Alexa A, Rahnenführer J, Lengauer T. Improved scoring of functional groups from gene expression data by decorrelating GO graph structure. Bioinformatics. 2006;22:1600–7.
80. Kassambara A. ggpubr: "ggplot2" Based Publication Ready Plots. 2023. Available from: https://rpkgs.datanovia.com/ggpubr/.
81. Taraporevala NF, Lesoway MP, Goodheart JA, Lyons DC. Precocious sperm exchange in the simultaneously hermaphroditic nudibranch, *Berghia stephanieae*. https://doi.org/10.1101/2022.03.02.482740.
82. Criswell KE, Gillis JA. Resegmentation is an ancestral feature of the gnathostome vertebral skeleton. Elife. 2020. https://doi.org/10.7554/eLife.51696.
83. Schindelin J, Arganda-Carreras I, Frise E, Kaynig V, Longair M, Pietzsch T, et al. Fiji: an open-source platform for biological-image analysis. Nat Methods. 2012;9:676–82.
84. Preibisch S, Saalfeld S, Tomancak P. Globally optimal stitching of tiled 3D microscopic image acquisitions. Bioinformatics. 2009;25:1463–5.
85. Towns J, Cockerill T, Dahan M, Foster I, Gaither K, Grimshaw A, et al. XSEDE: accelerating scientific discovery. Comput Sci Eng. 2014;16:62–74. https://doi.org/10.1109/mcse.2014.80.

Publisher's Note

Springer Nature remains neutral with regard to jurisdictional claims in published maps and institutional affiliations.